

The evolution of a localized nonlinear wave of the Kelvin–Helmholtz instability with gravity

Annagrazia Orazzo¹ and Jérôme Hoepffner²

¹*Department of Aerospace Engineering, DIAS, Università degli studi di Napoli Federico II, Italy*

²*UPMC Univ Paris 06 & CNRS, UMR 7190, Institut Jean Le Rond d'Alembert, F-75005 Paris, France*

(Received 23 February 2012; accepted 23 October 2012;
published online 29 November 2012)

At the interface between two fluids of different density and in the presence of gravity, there are well known periodic surface waves which can propagate for long distances with little attenuation, as it is for instance the case at the surface of the sea. If wind is present, these waves progressively accumulate energy as they propagate and grow to large sizes—this is the Kelvin–Helmholtz instability. On the other hand, we show in this paper that for a given wind strength, there is potential for the growth of a localized nonlinear wave. This wave can reach a size such that the hydrostatic pressure drop from top to bottom equals the stagnation pressure of the wind. This process for the disruption of the flat interface is localized and nonlinear. We study the properties of this wave using numerical simulations of the Navier–Stokes equations. © 2012 American Institute of Physics. [<http://dx.doi.org/10.1063/1.4767512>]

I. INTRODUCTION

A. Shear layers and self-similar solutions

An interface between two fluids of different velocity is subject to the Kelvin–Helmholtz instability. The first paper was that of Helmholtz.¹ He found that the origin of sound in the pipe organ was the instability and subsequent oscillation of a shear layer. He described this instability as the evolution of a localized irregularity on an infinitely thin shear layer: this localized irregularity would progressively roll-up into a spiral. A few years later, Kelvin² gave a description of this instability using the powerful mathematical framework of the low-amplitude sinusoidal perturbations. This description was successful in that he could predict explicitly the exponential growth rate of each wavelength. We should note here that the two approaches of Helmholtz and Kelvin are critically opposed: the one considers the nonlinear evolution of a localized perturbation, and the other considers the linear evolution of a periodic wave.

This critical opposition was the central topic of a recent article.³ In this paper, we performed numerical simulations of a shear layer and studied the differences between a weak sinusoidal initial condition (Kelvin) and a strong localized initial condition (Helmholtz). We have shown that in the case of a localized initial condition of amplitude sufficient to create immediately a nonlinear wave, we could observe a self-similar growth of the wave. The localized and nonlinear wave grows algebraically in time without changing its shape. This self-similar growth can be understood from the fact that the Euler equations have no intrinsic length scale, thus the only length scale is inertial $L = Ut$, with U the velocity jump across the shear layer and t the time. The wave grows self-similarly according to the growth of this inertial length scale. For the study of this localized wave in a different configuration, see Ref. 4. In the case of a sinusoidal initial condition on the other hand, such as the classical case of Kelvin's analysis, the self-similar growth cannot be observed since the periodic initial condition pollutes the dynamics with the scale of its wavelength: the dynamical structures appearing during the natural evolution of the instability (rolled-up vortices, also known as *Kelvin–Helmholtz billows*) are locked at this externally imposed wavelength. In the preface of his book

on scaling,⁵ Barenblatt explains why finding a self-similar solution is useful: “The statement that a certain phenomenon is *steady*, i.e., time independent, is obviously very significant: there is then no need to trace its evolution in time. Of similar significance is the statement that the phenomenon is *self-similar*.” We read also in Chap. II that “this behavior should be discovered, if it exists, and its absence should also be recognized.” In Ref. 3, we show that for two fluids of equal density, the self-similar solution consists in the winding of the shear layer into a couple of corotating vortices aligned at an angle of about 20° with the shear layer. When the density of the upper fluid is lowered, the self-similar solution loses its central symmetry and the vortex in the upper fluid gains in intensity whereas the vortex which was located in the lower fluid transforms into an elongated circulation bubble. The tip of the wave becomes unstable, oscillates like a flapping flag and sheds drops. For an even lower density of the upper fluid, the upper vortex detaches periodically in a typical vortex shedding sequence.

There are a few known self-similar solutions in relation with the behavior of mixing layers; these were studied mainly in the context of *vortex sheets*, that is, the limit in which the thickness of the layer tends to zero. Consider for instance the layer of vorticity in the wake of an airplane. At the tip of the wing, this layer tends to roll-up to form a large wing-tip vortex. The roll-up of this sheet can be described as a self-similar solution, known as the *Kaden roll-up*.⁶ Prandtl has shown also that a vortex sheet can conform in the shape of an infinite self-similar spiral, see Ref. 7. Prandtl’s solution was extended to multibranched spirals by Ref. 8, and these results were translated into the integro-differential formulation of the Birkhoff-Rott equation by Ref. 9. More recently, Ref. 10 developed a technique to solve numerically the self-similar equations: the equations describing the self-similar solutions of vortex sheet roll-up into spirals. This technique was applied to the computation of the Kaden roll-up. Evidence is shown in Ref. 11 of a family of self-similar roll-up with two vortices similar to the solution studied in Ref. 3 for the case with two fluids of equal density. Also, an early simulation of the evolution of the vortex sheet under a localized perturbation was performed in Ref. 12. A spiral roll-up is initiated locally upon an infinite shear layer. The aim was to describe the mechanism by which a localized vortex may feed from rolling up the sheet, possibly in a self-similar manner. Unfortunately, Ref. 11 shows that this single-vortex self-similar solution exists only for a sheet of spatially decreasing intensity. For a review, see Ref. 13.

The aim of the present paper is to pursue the analysis of the self-similar solution first observed in Ref. 11 with vortex sheets and later in Ref. 3 with direct numerical simulations. The self-similar solution is possible when there is no intrinsic length scale in the problem. If we chose to consider the effect of viscosity and surface tension, we add a viscous length scale and a capillary length scale. We can consider these scales as *small length scales*. When the instability is initiated locally, the wave may grow quickly beyond these two small length scales toward its self-similar regime: the bigger the wave, the lesser the impact of viscosity and capillarity; these two effects will play their role during the initial transient from the initial condition. In the case of a shear layer between two fluids of different densities and in the presence of gravity, there is yet another length scale, which is a *large length scale*: the bigger the wave the larger the impact of its weight. Our goal is to describe how the evolution of the wave is affected when it reaches a size where weight prevents its further growth.

B. Literature on Kelvin–Helmholtz instability

The literature on the shear layer instability is vast, and we would like to give a rapid overview of a sequence of papers relevant to our research.

Experimental measurements were made in Ref. 14 for the shear layer between miscible fluids and Ref. 15 for immiscible fluids; the shear layer is produced by tilting a container filled with two fluids of slightly different densities. The model for the growth of periodic waves was made assuming a constant amplitude of the wave in space: the *temporal stability analysis*. Another classical configuration for the shear layer is the flow downstream of a splitting plate. This plate separates two streams of different velocity, see Ref. 16.

The two articles^{17,18} have performed nonlinear analysis to show the first effects of nonlinearity, using expansions in the amplitude of the wave. It was shown that nonlinearities could be both stabilizing (saturation effect) or destabilizing. This destabilizing effect of nonlinearity may lead to a

subcritical instability behavior: the shear layer is stable to infinitesimal perturbations but unstable to finite size perturbations. The roll-up of the shear layer was also studied in the limit of an infinitely thin layer: the vortex sheet. It was shown by Ref. 19 that this roll-up leads to the creation of a curvature singularity in finite time. The location of this curvature jump is the birthplace of the vortex roll-up. The shear layer rolls into a spiral, which by means of viscosity diffuses into the rotating core of a vortex. The process of creation of these Kelvin–Helmholtz billows is described using numerical simulations in Ref. 20. Once a row of individual vortices are created from a periodic initial perturbation, they will themselves continue to evolve under the effect of mutual induction; we then observe the pairing of neighboring vortices, see Ref. 21.

The works described above consider periodic waves. On the other hand, excitation of the linear instability using a localized perturbation of low amplitude leads to the growth of a *wave packet*. This type of analysis retains the useful properties of the linearization while adding more information: we can see how the wave packet spreads in space. An early paper describing wave packets on shear layers is Ref. 22. This type of analysis became increasingly popular together with the notions of absolute and convective instability, see Refs. 23 and 24. With such tools, one can tell whether a packet of the unstable waves will grow while being advected away by the mean flow, or whether it will spread upstream and downstream to invade the shear layer.

The framework of wave packet analysis can be extended to look as well at the impact of nonlinearities. When a wave packet of initially low amplitude grows under the effect of the instability, it will reach amplitudes where nonlinear effects become important. There may thus be a nonlinear front progressing between the invading wave packet and the yet untouched shear-layer, see Ref. 25 for a theoretical article using the Ginzburg–Landau equation as an illustration, and Ref. 26 for an application of these ideas to wake flows.

In the present paper, we extend the study of the self-similar wave to the case where the gravity is present. This case is relevant to applications with density stratification. We find many realizations of such flow in geophysics: thermally stratified oceans for instance or in the atmosphere. This is also the case at the surface of the sea: the wind is blowing and waves may propagate and grow. The shear layer instability at a density jump will play an important role for mixing, see for instance Ref. 27 for an experimental paper. The case of the instability at the surface of the sea—very large density jump—was studied by Refs. 28 and 29. See as well Refs. 30 and 31 for theoretical analyses of the stability when the two fluids have different densities.

In this paper, we report our numerical experiments of a shear layer initially perturbed at a given location. A weak initial forcing would yield a wave packet growing and spreading and then becoming nonlinear. Instead, the initial force is large enough such as to create a wave immediately nonlinear. After a short initial transient, the wave tends to its self-similar regime of algebraic growth. Once the wave becomes large, the volume force of its weight starts to play its role against instability and against self-similarity as shown in Figure 1.

II. MODEL

Essentially, the wave is an obstacle to the gas stream such that the flow above its head is accelerated. This acceleration induces a pressure drop which is the driving force for the vertical growth of the wave. The intensity of this pressure drop does not depend on the size of the wave: this is the main ingredient for self-similarity. Since the wave grows, it will eventually reach a size at which volume forces such as gravity become comparable to the aerodynamic surface forces.

When does the wave stop growing? Once the hydrostatic pressure drop in the liquid body of the wave equals the aerodynamic pressure drop, there is no longer a driving power and the wave has reached its maximum size. Figure 1 displays the archetypal configuration: in gray the evolution of the weightless wave: growing in size without changing shape, in black the wave with gravity reach a stationary height after an initial transient. These simulations correspond precisely to the case and parameters of Ref. 3, except that a vertical acceleration is included to model gravity.

The main parameters are U the velocity difference between the gas and liquid, g the acceleration of gravity, ρ_{gas} and ρ_{liq} the densities of the gas and liquid (respectively, above and below the shear

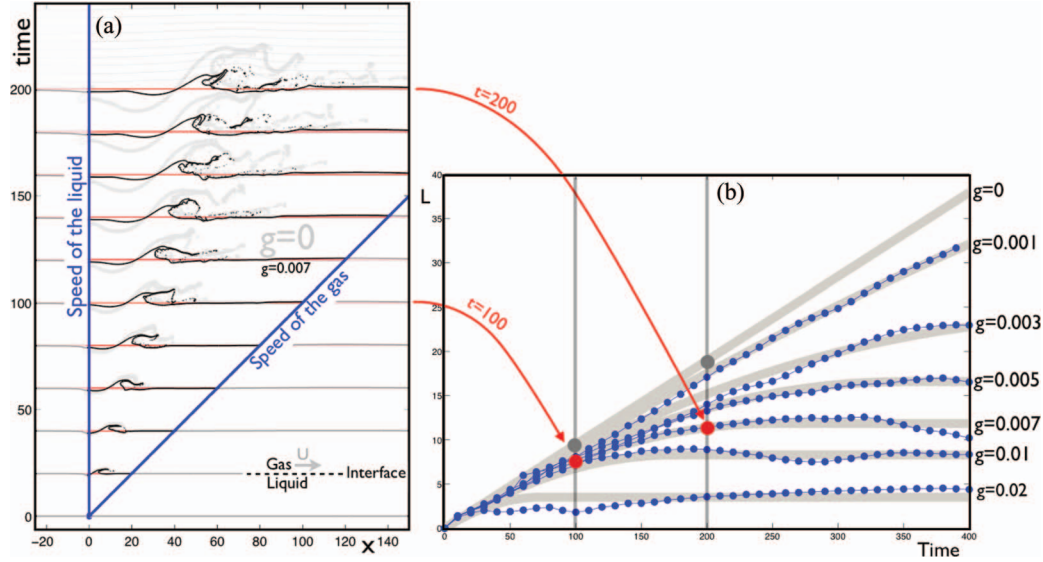


FIG. 1. (a) Evolution in time of the wave interface for a gas (fluid over the shear layer) ten times lighter than the liquid (the fluid below the shear layer) for a weightless wave $g = 0$ (light gray interface) and for $g = 0.007$ (black interface). (b) Evolution in time of the size of the wave while varying the intensity of the gravity.

layer). Dimensional analysis tells that the wave should reach its maximum size $L_{\text{apex}} \propto U^2/g$ in a time $T_{\text{apex}} \propto U/g$.

Once time and space are made nondimensional using these relevant scales, the remaining parameters are the Reynolds and the Weber numbers (quantifying, respectively, the effect of viscosity and surface tension), the ratio of the shear layer thickness and wave height δ/L_{apex} and the density ratio $r = \rho_{\text{gas}}/\rho_{\text{liq}}$. We may consider the ideal limit in which Reynolds and Weber numbers are large, and where the mixing layer is thin. The only remaining parameter is then the density ratio r .

We may now inspect the wave growth using a simple analysis based on the Bernoulli equation. See Figure 2 for a sketch of the wave configuration. The aerodynamic pressure drop due to the narrowing of the streamlines above the liquid obstacle is $\Delta p_{\text{gas}} \propto \rho_{\text{gas}} U^2$. In parallel, the pressure drop in the liquid due to the acceleration of the liquid sucked from its bottom at speed v and the gravity is $\Delta p_{\text{liq}} \propto \rho_{\text{liq}}(v^2 + gL)$. Since in the region of the wave head, the pressure is the same in the liquid and the gas, these two terms are equal yielding the suction velocity at the bottom of the wave

$$v^2 \propto rU^2 - CgL \quad (1)$$

with C a geometrical constant. This expression is characteristic of the counteracting effects of inertia and weight: the second term is growing with wave size L . Now, the law describing the evolution of the wave size can be simply obtained: considering that the wave area grows in time proportionally

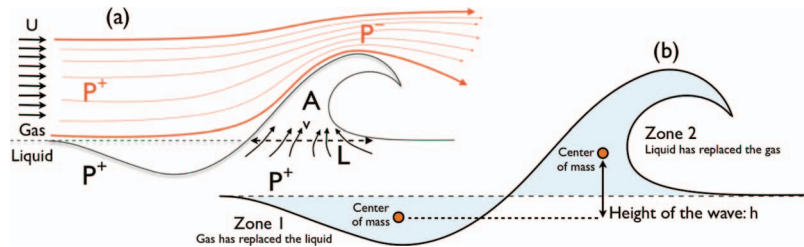


FIG. 2. Schematic representation of the growing wave. (a) Illustration of the streamline and pressure relevant to the dynamic model of the wave (1), and (b) wave structure used to define the height of the wave from consideration of its gravity potential energy in (4).

to the amount of the liquid sucked at speed v from the bottom section of the wave of length L , we get $\dot{L} \propto v$, which yields upon integration

$$\overbrace{L = a\sqrt{r}Ut - bgt^2}^{\text{Weightless law}}, \quad t < T_{apex} \quad (2)$$

$$L = L_{apex}, \quad t \geq T_{apex}.$$

We recognize the weightless algebraic growth for short times, with the constant a , which is counteracted with a gravity term growing like the square of time, until $t = T_{apex}$ where it forbids any more growth, after this threshold time, our simple analysis predicts that the wave keeps its maximum size L_{apex}

$$L_{apex} = \alpha r \frac{U^2}{g}, \quad T_{apex} = \beta \sqrt{r} \frac{U}{g} \quad (3)$$

with $\alpha = a^2/4b$, $\beta = a/4b$.

This law of growth and saturation of the wave under the combined action of wind and weight is compared to computed data in Figure 1(b)). We show the evolution in time of the wave size while varying g from 0 (the self-similar evolution) up to $g = 0.02$. Superimposed to the numerical data we have drawn (2) with constant a adjusted on the weightless algebraic law, and b such as to fit best the data for all shown values of g . We can see indeed that all curves start with the same slope as the weightless case, and saturate at a height compatible with the scaling on U^2/g from (3).

The integration in (3) predicts an evolution of the wave in two sequences, first a growth where the algebraic law of the weightless wave is progressively compensated with a gravity term growing like the square of time, followed by a state with a wave of constant size. The behavior of this model could indicate the sequence of birth of a dissipative soliton, producing a steady wave as the equilibrium of a destabilizing aerodynamic force and a stabilizing weight.

A. How to measure the height of the wave

As can be seen in Figure 1, the weightless wave has globally a self-similar growth, but it is constantly disturbed by local instabilities and instationarities most obvious as the flapping of its tongue. On the other hand, our quantitative model is crude in the sense that it only describes the global behavior of the liquid structure. We thus need to choose an observable which is witness of this global behavior of the structure and overlooks the small scale details. In the paper without gravity,³ we chose to extract a measure of the wave size from the area A of liquid which has crossed through the initial position of the interface $y = 0$. This is an integrated quantity whose square root can be considered an adequate measure of the wave size.

This choice of an observable was appropriate in the case of the self-similar wave since its aspect ratio does not change in time. The algebraic law for \sqrt{A} was thus a suitable way to test the theory. In the case of the wave with gravity on the other hand, a strong anisotropy is introduced which prevents the wave from growing in the vertical direction; we thus need a new observable to measure the height of the wave. We could choose to record the evolution in time of the highest liquid particle, but this measure will wildly fluctuate with the flapping and shedding of drops: it is preferable once again to consider an integrated quantity.

Since the wave is growing against the action of gravity, we may devise a measure inspired from considerations of the gravity potential energy of the liquid system. The gravity potential energy of a fluid element at altitude y is $dE_p = \rho gy dS$. Thus the variation of total gravity potential energy from initial time to time t is

$$\Delta E_p = g \int_{xy} [\rho(x, y, t) - \rho(x, y, 0)] y dS.$$

The density ρ in this equation can be either that of the liquid or that of the gas. Considering an arbitrary point x, y in space, the contribution of this point to the integral is zero if the fluid has not changed from time 0 to time t . We may thus define two zones who contribute to this variation of

energy: zone 1 where gas has replaced the liquid, and zone 2 where liquid has replaced the gas, see Figure 2. The change of potential energy is thus

$$\Delta E_p = g \int_1 (\rho_{gas} - \rho_{liq}) y dS + g \int_2 (\rho_{liq} - \rho_{gas}) y dS,$$

which we can rewrite

$$\Delta E_p = g(\rho_{liq} - \rho_{gas}) \left(\underbrace{\int_2 y dS}_{Ah_2} - \underbrace{\int_1 y dS}_{Ah_1} \right) = g(\rho_{liq} - \rho_{gas}) Ah, \quad (4)$$

where A is the surface of the zones (the two surfaces are equal due to conservation of volume) and h_1 and h_2 are the altitudes of the center of mass of zones 1 and 2. This last expression shows that $h = h_2 - h_1$ is a measure of the wave height relevant in terms of the potential energy related to gravity. This is the measure that we will use to test our theory for the plateau induced by gravity.

B. Numerical experiments

We saw in Figure 1 that the behavior of the wave is compatible with the scaling on Froude number for $r = 0.1$, that is, for a gas ten times lighter than the liquid. We would like now to complete the study and validate the scaling law in density ratio.

In the theoretical analysis of Sec. II, we have considered the ideal limit where Reynolds and Weber numbers are large, and the limit where the thickness δ of the mixing layer is small. As usual, asymptotic limits are relevant for the understanding of physical processes only if the conclusion that can be drawn in this ideal setting remain approximately valid for finite values of the nondimensional numbers. This is what we would like to test here. Our tool of experimentation is numerical simulations of the Navier–Stokes equations for a system of two interacting fluids. Memory and computation time limitations impose moderate values of the Reynolds, Weber, and δ . So it will be convenient to adopt a different dimensionalization than in Ref. 3 for our simulations. We have chosen U^2/g and U/g as reference length and time, and vary the density ratio r while keeping the Reynolds and Weber fixed. Also, the initial mixing layer thickness is given its value in proportion of the predicted maximum wave size.

We use the open source software Gerris Flow Solver.³² Sizes are made nondimensional using the reference size U^2/g and times with U/g , equivalent to taking $U = g = 1$ in our simulations. In preliminary computations we found that the top of the liquid wave reaches approximately the height $L_{apex} = 0.7rU^2/g$ in time $T_{apex} = 5\sqrt{r}U/g$, so we set the parameters in proportion to these references. The box height is $8L_{apex}$ to avoid confinement from the boundary conditions, while retaining the resolution of the wave when it reaches its plateau. The box is four time longer than high. The initial shear layer thickness δ is set to $L_{apex}/20$. The viscous law of diffusion of the *error function* velocity profile is $\text{erf}(y/2\nu(t - t_0))$ with ν the kinematic viscosity of each fluid. The viscosity is set in each fluid such that the mixing layer thickness is multiplied by 3 by viscous growth at time T_{apex}

$$\nu = 4\delta^2/T_{apex}.$$

This choice of viscosity gives a Reynolds based on δ of $\approx 36/\sqrt{r}$, thus ≈ 110 for $r = 0.1$ and ≈ 360 for $r = 0.01$. The Reynolds based on L_{apex} is 20 times these values: 2200 and 7200. Surface tension σ is chosen such that the Weber number $We = \rho_{gas}\sigma U^2/L_{apex}$ is 500.

The software affords adaptive grid refinement based on vorticity and interface curvature. Here the smallest mesh size is 2^{-10} times the box height, amounting to 128 mesh cells in the wave height L_{apex} . We have performed extensive grid resolution studies in our previous work,³ and we found that this mesh spacing was sufficient to ensure convergence of the measurements extracted from the wave: its size and height evolving in time.

The initial condition is a parallel mixing layer satisfying the continuity of velocity and shear strain at the interface location $y = 0$

$$u(y) = \begin{cases} \frac{1}{1+r}(\text{erf}(y/\delta) + r), & y > 0 \\ \frac{r}{1+r}(\text{erf}(y/\delta) + 1), & y < 0. \end{cases}$$

This velocity field is initially disturbed by a local vertical acceleration

$$f(x, y, t) = \kappa\phi(t) \exp(-(x/\ell)^2 - (y/\ell)^2)$$

with its amplitude quickly fading

$$\phi(t) = \begin{cases} \cos(\pi t/2t_{stop}) & t < t_{stop} \\ 0, & t > t_{stop}. \end{cases}$$

We took $\ell = \delta$ a forcing patch of the size of the mixing layer, and $t_{stop} = T_{apex}/100$. The amplitude of the forcing is $\kappa = 0.1/t_{stop}$.

For the present study we have chosen to consider a 2D simulation of the wave growth. This choice may be questionable at first sight since the creation of the droplets of a spray must ultimately be a three-dimensional process. This is indeed shown in Ref. 33: atomization starts with the creation of liquid films which destabilize into liquid ligaments, and which in turn are finally segmented into droplet by the Rayleigh–Plateau instability. In the present work, we focus at the scale of the creation of the liquid film; this is clear from the choice of a large Weber number of 500. The Kelvin–Helmholtz instability acts such as to build the localized wave, with its tip and flapping tongue. This tongue is fragile, since it is only weakly maintained by surface tension. It is stretched with the air flow, away from the body of the wave and shaken by the vortices that are shed periodically from the liquid obstacle. Segmentation in our 2D simulations happens artificially when the two interfaces of the liquid film meet into a single computational cell, that is, at a size 128 times smaller than the wave itself. In terms of the global scaling we wish to demonstrate here, whether the liquid carried up is finally observed as a liquid film or as droplet has little impact. At this stage indeed, the wind has already played its part against the attraction of gravity.

What could be the 3D effects acting at the scale of the wave? Wave breaking under gravity is mostly a 2D process; the lateral localization we can observe at sea is mainly a consequence of several oblique wave trains interacting by addition and cancellation. Another candidate for a 3D effect is the lateral destabilization of the Kelvin–Helmholtz billows, as discussed in Ref. 20. This secondary instability can be observed when the mixing layer has already rolled into vortices: when the Kelvin–Helmholtz is no longer active and strong. This effect is much weaker than the Kelvin–Helmholtz instability itself.

C. Impact of the density ratio

We show the evolution of the wave interface in Figure 3 for four successive times. The first one is $T_{apex}/10$ where we can see the start of the wave as the result of the initial localized impulse. The wave has not taken yet its own distinctive shape. This is a time of the initial transient, where the cause of the wave is not yet forgotten. The second interface corresponds to $T_{apex}/2$, half way on the growth of the wave to reaching its peak height. Already at this time, we can observe the flapping of the wave's tongue and shedding of a liquid film. At $t = T_{apex}$, the wave has reached its maximum height, with a value corresponding approximately to $L_{apex} = 0.7rU^2/g$, materialized on the four graphs as a horizontal dashed line. At this time of largest size, we see that there has already been a strong activity of shedding liquid films and drops, some of which have free-fallen down to the original interface height. The last displayed interface position corresponds to $t = 1.5T_{apex}$. We mentioned in Sec. II that the theoretical analysis left the possibility for a behavior of this wave as a dissipative soliton. We can see here that this is in fact not the case: after reaching its maximum size, the wave collapses progressively, losing its impetus into an intricate organization of vortices and drops.

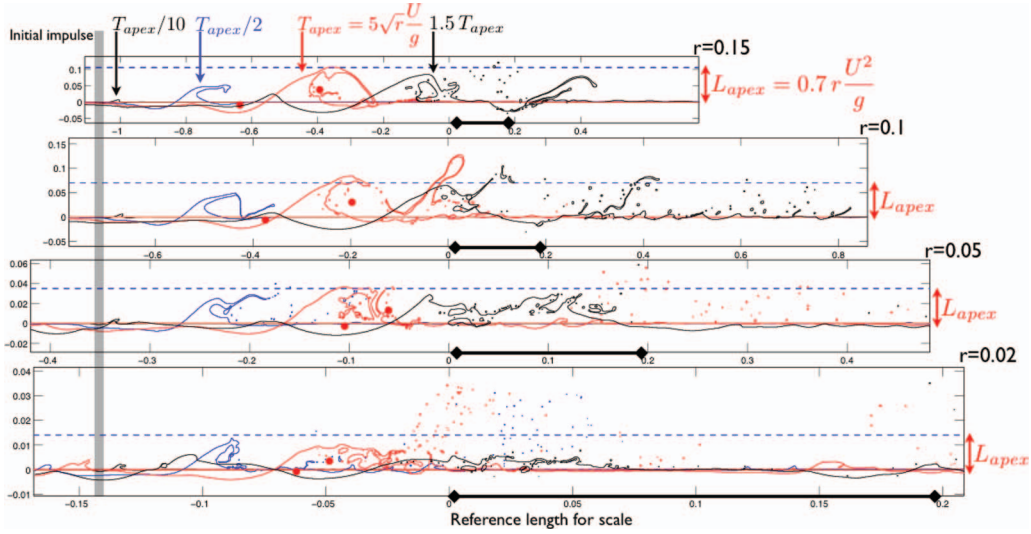


FIG. 3. Position of the interface from numerical simulations at four instants of time and for four values of the density ratio. Relative sizes are scaled such as to emphasize the theoretical prediction. The positions of the center of mass of zones 1 and 2 at time T_{apex} are drawn as dots (red online).

The graphs for the four values of the density ratio r are displayed scaled such as to emphasize the theoretical scaling law. We can observe that the shape and behavior does not change significantly once properly scaled, at least for the values of r which we were able to simulate. The most significant difference comes from the behavior of shed drops downstream of the wave. Indeed, the present choice of the Weber number based on the gas speed U does not account for the fact that the wave has a slower speed as r is lowered, see Ref. 3 for a discussion. Thus the shearing power of the free-stream upon the tensed interface is larger for the lower gas densities. The second reason for difference in the drop behavior comes from the fact that once the drops have left the liquid wave, they are advected at the free-stream velocity while free-falling with little or no influence from the density ratio.

The effect of the density ratio on the wave height is displayed in Figure 4. The size of the wave is quantified using the measure inspired from the variation of the gravity potential energy h as described in Sec. II A. We can observe the initial growth of the wave height. Here we would have expected initially different slopes for the growth of the wave, in agreement with the algebraic law for the self-similar growth as shown on Figure 1. This is not observed here since with the present choice of parameters due to mesh size limitations, the wave unfortunately does not have time to

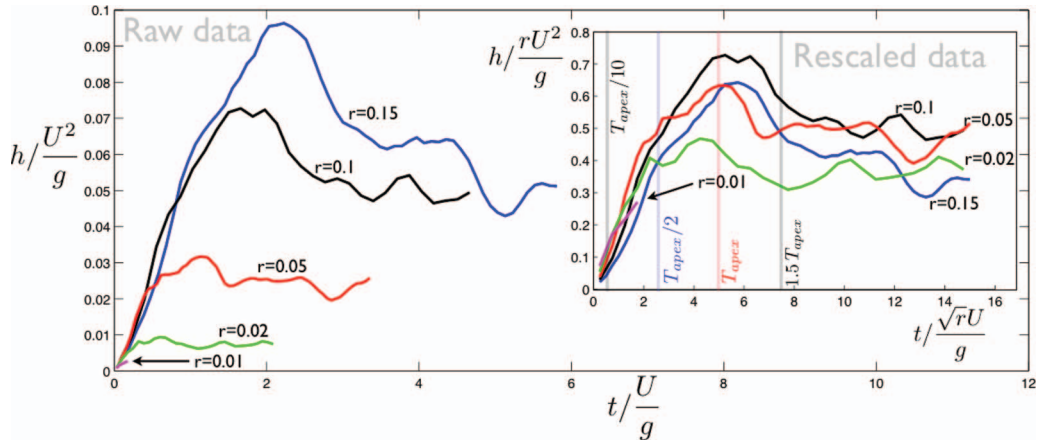


FIG. 4. Effect of the density ratio on the evolution of the height of the wave. Inset: height and time are scaled with their theoretical values for the plateau.

realize its self-similar regime before reaching the size at which volume forces start to act. After this initial growth, the height shows a peak and subsequent decay as expected from the progressive collapse seen in Figure 3 after the apex. The simulation performed for the smallest value of the density ratio $r = 0.01$, a gas hundred times lighter than the liquid could not complete to time T_{apex} and does not show the peak. The computation is being made increasingly difficult as the fluids have strongly different physical properties.

The test of the model for the wave growth is shown in the inset of Figure 4; the scaling of the time as

$$t' = \frac{t}{\sqrt{rU/g}} \quad \text{and height as } h' = \frac{h}{rU^2/g}$$

yields a gathering of the time evolution of the wave height for the five values of the density ratio, showing a coordinated behavior of the physical system as the density of the gas is progressively lowered. The plateau value for h' is about 0.45, and the peak is observed at a time t' of about 5.

III. DISCUSSION

We have extended the theory for a self-similar behavior of the Kelvin–Helmholtz instability, and elaborated a model for a nonlinear wave of gravity and wind. The wave initially grows until reaching a size at which gravity can counterbalance the destabilizing effect of the aerodynamic pressure drop.

It would have been fortunate if this wave had been the dissipative soliton of wind and gravity which the idealized model (2) had left us to hope for. Indeed, once the hydrostatic pressure drop balances the aerodynamic pressure drop, there is potentiality for a steady wave. On the other hand, the dynamic processes at play are not structurally stable in the connection of the liquid body and the deflected air stream, such that a progressive collapse follows the apex of the growth. The model nevertheless provides insight into the growth process itself since the data for varying density ratio are reasonably gathered by the scaling of time as the square root of the density ratio and height as the density ratio in Figure 4. Could we have proposed a more accurate quantitative law? The simulations of this two-phase flow are demanding; violent drop impacts and shedding are prone to cause numerical instabilities for low density ratio. Figure 3 is eloquent of the complexity of the system, and we must be content in this first study with the predictive ability of such a trimmed quantitative account as (2).

To conclude, we may say that there is one kind of wave which is well known, a periodic deformation of the interface. We know that this kind of wave—for instance at the surface of the sea—may travel on very long distances, and that it can grow to a large size under the effect of a strong wind. This description of such waves is essentially linear or weakly nonlinear. When a given wavelength is led to grow in amplitude, the aspect ratio of the wave may grow to such an extent that the crest of the wave starts to break, leading to dissipation of energy in a process of saturation. This breaking creates foam and spray at the crest, see Ref. 34.

We may on the other hand think of what happen at the surface of the sea from an alternative point of view. At a given wind velocity, there is a potential for a pressure drop $\alpha \rho_{\text{gas}} U^2$ with α a geometric factor originating in the pattern of streamlines. This pressure can be responsible of an elevation of the liquid surface to a height h corresponding to the hydrostatic pressure drop $\rho_{\text{liq}}hg$. The question *what would such a wave look like?* is just what we have tried to answer in this paper. To allow for analysis, we have considered the simplified setting of a flat interface and a localized initial impulse. This wave shall look like Figure 3, it ejects much of its liquid body into airborne drops, and we found that the numeric factor α is of order one. In order to emphasize the difference with surface waves which slowly accumulate energy, we may call such a wave a *spontaneous storm wave*.

¹ H. Helmholtz, “On discontinuous movements of fluids,” *Philos. Mag. (Ser. 4)* **36**, 337–346 (1868).

² W. Thomson, “Hydrokinetic solutions and observations,” *Philos. Mag. (Ser. 4)* **42**, 362–377 (1871).

³ J. Hoepffner, R. Blumenthal, and S. Zaleski, “Self-similar wave produced by local perturbation of the Kelvin–Helmholtz shear-layer instability,” *Phys. Rev. Lett.* **106**(10), 104502 (2011).

- ⁴ A. Orazzo, G. Coppola, and L. de Luca, "Single-wave Kelvin-Helmholtz instability in nonparallel channel flow," *Atomization Sprays* **21**(9), 775–785 (2011).
- ⁵ G. I. Barenblatt, *Scaling* (Cambridge University Press, Cambridge, 2006).
- ⁶ H. Kaden, "Aufwicklung einer unstabilen unstetigkeits flache," *Ing.-Arch.* **2**, 140 (1931).
- ⁷ L. Prandtl, "Über die entstehung von wirbeln in der idealen flüssigkeit (1922)," in *Gessamme abhandlungen* (Springer, Berlin, 1961), Vol. 2, pp. 697–713.
- ⁸ R. C. Alexander, "Family of similarity flows with vortex sheets," *Phys. Fluids* **14**, 231 (1971).
- ⁹ T. Kambe, "Spiral vortex solution of Birkhoff-Rott equation," *Physica D* **37**, 463–473 (1989).
- ¹⁰ D. I. Pullin, "The large scale structure of unsteady self-similar rolled-up vortex sheets," *J. Fluid Mech.* **88**(3), 401–430 (1978).
- ¹¹ D. I. Pullin, "On similarity flows containing two-branched vortex sheets," in *Mathematical Aspects of Vortex Dynamics*, edited by R. E. Caflisch (Society for Industrial and Applied Mathematics, Philadelphia, 1989), pp. 97–106.
- ¹² J. Jimenez, "Numerical simulation of mixing layer vortices," in *Structure and Mechanisms of Turbulence I*, Lecture Notes in Physics Vol. 75, edited by H. Fiedler (Springer, Berlin/Heidelberg, 1978), pp. 147–161.
- ¹³ P. G. Saffman and G. R. Baker, "Vortex interactions," *Annu. Rev. Fluid Mech.* **11**, 95–122 (1979).
- ¹⁴ S. A. Thorpe, "Experiment on the instability of stratified shear flows: miscible fluids," *J. Fluid Mech.* **46**(2), 299–319 (1971).
- ¹⁵ S. A. Thorpe, "Experiments on the instability of stratified shear flows: immiscible fluids," *J. Fluid Mech.* **39**, 25–48 (1969).
- ¹⁶ G. L. Brown and A. Roshko, "Density effects and large structure in turbulent mixing layers," *J. Fluid Mech.* **64**, 775 (1974).
- ¹⁷ J. T. Stuart, "On finite amplitude oscillations in laminar mixing layers," *J. Fluid Mech.* **29**(Part 3), 417 (1967).
- ¹⁸ J. W. Miles, "Weakly nonlinear Kelvin-Helmholtz waves," *J. Fluid Mech.* **172**, 513–529 (1986).
- ¹⁹ D. W. Moore, "The spontaneous appearance of a singularity in the shape of an evolving vortex sheet," *Proc. R. Soc. London, Ser. A* **365**, 105–119 (1979).
- ²⁰ P. C. Patnaik, F. S. Sherman, and G. M. Corcos, "Numerical-simulation of Kelvin-Helmholtz waves of finite-amplitude," *J. Fluid Mech.* **73**, 215–240 (1976).
- ²¹ C. D. Winant and F. K. Browand, "Vortex pairing: the mechanism of turbulent mixing-layer growth at moderate Reynolds number," *J. Fluid Mech.* **63**, 237 (1974).
- ²² M. A. Weissman, "Non-linear wave packets in the Kelvin-Helmholtz instability," *Philos. Trans. R. Soc. London, Ser. A* **290**(1377), 639–681 (1979).
- ²³ C.-M. Ho and P. Huerre, "Perturbed free shear layers," *Annu. Rev. Fluid Mech.* **16**, 365–424 (1984).
- ²⁴ P. Huerre and P. A. Monkewitz, "Local and global instabilities in spatially developing flows," *Annu. Rev. Fluid Mech.* **22**, 473–537 (1990).
- ²⁵ A. Couairon and J. M. Chomaz, "Absolute and convective instabilities, front velocities and global modes in nonlinear systems," *Physica D* **108**(3), 236–276 (1997).
- ²⁶ B. Pier and P. Huerre, "Nonlinear self-sustained structures and fronts in spatially developing wake flows," *J. Fluid Mech.* **435**, 145–174 (2001).
- ²⁷ E. J. Strang and H. J. S. Fernando, "Entrainment and mixing in stratified shear flows," *J. Fluid Mech.* **428**, 349–386 (2001).
- ²⁸ J. W. Miles, "On the generation of surface waves by shear flows," *J. Fluid Mech.* **3**(2), 185–204 (1957).
- ²⁹ J. W. Miles, "On the generation of surface waves by shear flows. 3. Kelvin-Helmholtz instability," *J. Fluid Mech.* **6**(4), 583 (1959).
- ³⁰ G. I. Taylor, "Effect of variation in density on the stability of superposed streams of fluid," *Proc. R. Soc. London, Ser. A* **132**(820), 499–523 (1931).
- ³¹ S. A. Maslowe and J. M. Thompson, "Stability of a stratified free shear layer," *Phys. Fluids* **14**(3), 453 (1971).
- ³² S. Popinet, "An accurate adaptive solver for surface-tension-driven interfacial flows," *J. Comput. Phys.* **228**, 5838–5866 (2009).
- ³³ J. Eggers and E. Villermaux, "Physics of liquid jets," *Rep. Prog. Phys.* **71**, 036601 (2008).
- ³⁴ S. R. Massel, *Ocean Waves Breaking and Marine Aerosol Fluxes* (Springer, New York, 2007).